An Optimal Control Strategy Design for Plug-in Hybrid Electric Vehicles Based on Internet of Vehicles

Yuanjian Zhang[1], Yonggang Liu[2], Yanjun Huang[3], Zheng Chen[4, 5*], Guang Li[5], Wanming Hao[6*], Geoff Cunningham[1], and Juliana Early[1]

[1]School of Mechanical and Aerospace Engineering, Queen's University of Belfast, BT9 5AG, Northern Ireland.

[2]State Key Laboratory of Mechanical Transmission & School of Automotive Engineering, Chongqing University, Chongqing, 400044, China

[3]School of Automotive Studies, Tongji University, 12476 Shanghai, Shanghai, 201804, China

[4]Faculty of Transportation Engineering, Kunming University of Science and Technology, Kunming, 650500, China

[5]School of Engineering and Materials Science, Queen Mary University of London, London, E1 4NS, UK

[6]School of Information Engineering, Zhengzhou University, Zhengzhou, 450003, China

Corresponding Authors: Zheng Chen (chen@kust.edu.cn) and Wanming Hao (iewmhao@zzu.edu.cn)

Abstract: This paper presents an approach to the design of an optimal control strategy for plug-in hybrid electric vehicles (PHEVs) incorporating Internet of Vehicles (IoVs). The optimal strategy is designed and implemented by employing a mobile edge computing (MEC) based framework for IoVs. The thresholds in the optimal strategy can be instantaneously optimized by chaotic particle swarm optimization with sequential quadratic programming (CPSO-SQP) in the mobile edge computing units (MECUs). The vehicle-to-vehicle (V2V) and vehicle-to-infrastructure (V2I) communication are adopted in IoV to collect traffic information for a CPSO-SQP based optimization and transmit the optimized control commands to vehicle from MECUs. To guarantee real-time optimal performance, the communication delay in V2V and V2I is decreased via an alternative iterative optimization algorithm (AIOA) approach. The simulation results demonstrate the superior performance of the novel optimal control strategy for PHEV with 9% improvement, compared with the original strategy.

Key words: Optimal control strategy, plug-in hybrid electric vehicle (PHEV), Internet of Vehicles (IoVs), mobile edge computing (MEC), chaotic particle swarm optimization with sequential quadratic programming (CPSO-SQP), alternative iterative optimization algorithm (AIOA).

I. INTRODUCTION

The 5th generation communication technology offers the potential for rapid developments in the field of Internet of Vehicles (IoVs) [1]. In highly evolved IoVs, the frequency of information interchange, information carrying capacity and other essential parameters are highly evolved to the point where they can facilitate novel vehicle-environment cooperation methods, such as mobile edge computing (MEC) [2]. Using these platforms,

further energy saving opportunities beyond that achievable from the information available to an isolated vehicle can be identified, and this opportunity is explored in this work for plug-in hybrid electric vehicles (PHEVs). Here, we focus on the optimal design of a control strategy for the studied 4-wheel drive (4WD) PHEV and how this can be improved through leveraging IoV capability. The mode of operation and energy management are the two key factors that impact on fuel economy. To this end, there have been numerous studies undertaken considering strategies for minimization of energy consumption in PHEVs. These methods can be divided into the following three categories according to the characteristics of different algorithms: rule based strategies [3, 4], global optimization based strategies [5, 6], and instantaneous optimization based strategies [7, 8].

Rule based strategies, such as threshold strategies [9] and fuzzy logic based strategies [10], can typically be implemented in real time as they have relatively low computational intensity. However, the threshold values or rules are normally designed by expert knowledge and therefore can be difficult to adapt to various driving conditions. Global optimization based strategies, such as dynamic programming (DP) [11], can be used to develop optimal control rules offline, but this process is typically computationally intensive and again does not lend itself to real time adaptability. While there are options for instantaneous optimization which can offer reasonable real time performance, but still do not provide the level of responsiveness that would be desirable in a fully adaptive system. Reinforcement learning [12] and deep reinforcement learning methods [13] have emerged as promising candidates, and have been shown potential in development of mode transition strategies and energy distribution management in PHEVs. However, these methods again place high computational demands on vehicle hardware. Moreover, in most of the proposed methods, mode transition and energy distribution are undertaken simultaneously by calculating the appropriate energy distribution ratio. This may lead to frequent mode transition, owing to the limitations of the different linear and non-linear optimization algorithms. It is thus imperative to look back upon the simple rule based method with optimally determined threshold values for respective mode transition and energy management by incorporating environment information via IoVs. Through this strategy, some restrictions of traditional rule based methods, caused by pseudo-expert knowledge, can be overcome, thus allowing the system to become more responsive to time-varying driving conditions.

However, the implementation of real-time control strategies in IoVs still has challenges. Due to the limited computational capacity of most mobile devices, many of the proposed control strategies for PHEVs require longer

computational time than the time step that would be permissible for safe vehicle control, which again presents a barrier to achieving real-time flexibility, and cloud computing capabilities typically rely on servers located far from the vehicle. As such, MEC, where the computation is undertaken at the edge of a mobile network (for instance, through local servers) has the potential to reduce network congestion and latency overcoming many of these limitations [14]. By this way, the complex onboard control processes can be executed at network edge, instead of in on-board VCU. In this case, the vehicle needs to offload the optimization task (either in part or fully) to network edge via a wireless network. The offload rate, also known as the communication rate, can be evaluated for its suitability by measuring the communication delay. In recent years, considerable progress has been made in millimeter wave (mmWave) with ultra-wide bandwidth technologies [15], whose implementation is based on the sparse radio frequency (SRF) chain antenna structure at the edges of the vehicle and the base stations (BSs) of network. It is anticipated that this will lower hardware costs and associated power consumption [16] relative to other communication methods, and the SRF chain antenna structure could be adopted in MEC to provide the necessary communication rates.

Motivated by these technology advancements, a multi-dimension optimization based novel control strategy is proposed in this study for a 4WD PHEV to exploit the capability of MEC based framework. An online control threshold optimization method based on the chaotic particle swarm optimization with sequential quadratic programming (CPSO-SQP) is applied, in which the control thresholds are instantaneously tuned via the MEC based vehicle-environment cooperation in IoVs. The MEC based framework empowers efficient energy management accomplished in real time by integrally utilizing powerful computation capabilities of different control modules. To guarantee optimal control effect, the communication speed, commonly indexed by communication delay, among different control modules in MEC based framework should be guaranteed. Therefore, the communication delay in the MEC based framework is optimized by studying a joint optimization problem of the precoding design under SRF chain antenna structure and offloading task. Three contributions are added in the literature:

1. A MEC based cooperative control framework is constructed. The cooperation among vehicle on-board VCU, mobile edge computing units (MECUs) and global server make it possible to attain the efficient vehicle-environment cooperative control by virtue of IoV.

2. The CPSO-SQP is employed to instantaneously optimize the control thresholds of the proposed strategy in MECUs, which assimilates the traffic information processed by the MEC and identifies the most appropriate control thresholds in the given route segment. The CPSO-SQP prompts the control effect of original strategy by adding the optimization skills into the expert-knowledge based strategy design. The off-vehicle optimization manner, additionally, strengthens the capability of the novel strategy in real-time application.
3. The communication delay in the MEC based framework, including delay in vehicle-to-vehicle (V2V) and vehicle-to-infrastructure (V2I), is reduced exhaustively through the joint optimization by employing the alternatively iterative optimization algorithm (AIOA). The reduced communication delay enables that complex control tasks can be instantly and flexibly shared among different computation resources in MEC based cooperative control framework, thereby strengthening the capacity of real-time application of the raised control strategy and enhancing improvement of fuel economy.

The remainder of this study is organized as follows. The studied 4WD PHEV, original control strategy and designed optimal control strategy are described in Section II. Section III elaborates on the CPSO-SQP based method which has been used here to optimize the control thresholds. Section IV provides the AIOA to prompt the communication ability. Section V discusses the simulation results and discusses the performance of the new control optimization approach developed here relative to traditional methods for control threshold optimization, followed by the main conclusions drawn in Section VI.

II. The Studied 4WD PHEV and Designed Optimal Control Strategy

The studied 4WD PHEV, as illustrated in Fig. 1, consists of an internal combustion engine (ICE), generator, motor 1 and motor 2. The specific hybrid powertrain can operate in several different modes by cooperatively controlling the ICE, generator and motors, providing extreme drivability and greater potential in energy savings when compared with the two-wheel drive (2WD) PHEV. Motor 1 and motor 2 are installed on the front and rear axle, respectively. The ICE can either drive the vehicle directly with motors in parallel mode or supply tractive power through driving the generator in serial mode. The ICE and generator are known collectively as the auxiliary power unit (APU) in serial mode. The switch between serial and parallel mode is achieved by controlling the engagement/disengagement of the clutch between the ICE and motor 1. Additionally, the 4WD PHEV can also operate in pure electric (EV) mode and is driven by motor 1 and motor 2 together. In this paper, the torque

distribution ratio between motor 1 and motor 2 is fixed at 0.5. The original logic of controlling the mode transition in the studied PHEV has been designed by a rule-based method based on the data from a benchmark test. The mode switch is chosen according to the current vehicle speed v, the required tractive power P_{req} and the required tractive torque T_{req}. The mode transition conditions are illustrated in Fig. 2.

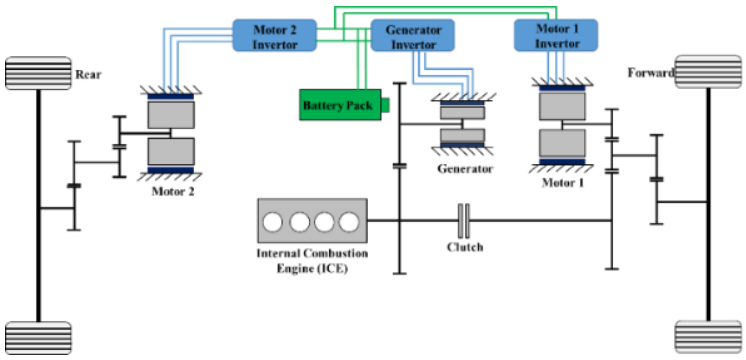

Fig. 1. The schematic of the 4WD PHEV configuration.

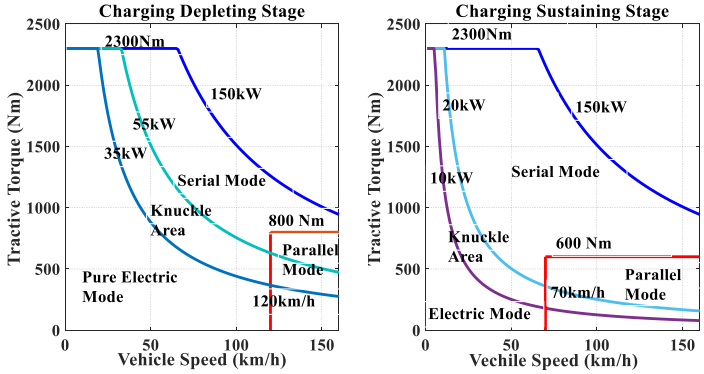

Fig. 2. Mode transition conditions in charge-depleting and charge-sustaining stage.

In general, the original energy management principle is to regulate the engine to operate in the brake-specific fuel consumption (BSFC) line based on the load following method. The energy management in both serial and parallel mode at charge-depleting and charge-sustaining stage can be shown in Tables 1 and 2.

Table 1 Energy management principle in charge depleting and sustaining stages under the serial mode

$P_{req} < P_{apu\_opt}$	$P_{apu} = 0$	$P_{batt} = P_{req}$
$P_{apu\_opt} \le P_{req} < (P_{apu\_opt} + P_{batt\_\max\_CD/CS\_s})$	$P_{apu} = P_{apu\_opt}$	$P_{batt} = P_{req} - P_{apu\_opt}$
$(P_{apu\_opt} + P_{batt\_max\_CD/CS\_s}) < P_{req}$	$P_{apu} = P_{apu\_max}$	$P_{batt} = P_{req} - P_{apu\_opt}$

Table 2 Energy management principle in charge depleting and sustaining stage under the parallel mode

$P_{req} < P_{eng\_opt}$	$P_{eng} = 0$	$P_{batt} = P_{req}$
$P_{eng\_opt} \le P_{req} < (P_{eng\_opt} + P_{batt\_\max\_CD/CS\_p})$	$P_{eng} = P_{eng\_opt}$	$P_{batt} = P_{req} - P_{eng\_opt}$
$(P_{eng\_opt} + P_{batt\_max\_CD/CS\_p}) < P_{req}$	$P_{eng} = P_{eng\_max}$	$P_{batt} = P_{req} - P_{eng\_opt}$

where P_{apu_opt} and P_{eng_opt} denote the power corresponding to the optimal operation points of APU; P_{apu_max} and P_{eng_max} denote the maximum power corresponding to the specific speed of APU and ICE; $P_{batt\_max\_CD\_s}$ and $P_{batt\_max\_CS\_s}$ correspond to the maximum power limit of battery in the charge-depleting and charge-sustaining stage when the vehicle is in serial mode; $P_{batt\_max\_CD\_p}$ and $P_{batt\_max\_CS\_p}$ correspond to the maximum power limit of battery in charge-depleting and charge-sustaining stage when the vehicle is in parallel mode. The APU integrating ICE and generator operates to output tractive power in serial mode. P_{apu_opt} is calculated based on the combined efficiency look-up table data of the ICE and generator, and P_{eng_opt} is calculated based on the ICE efficiency look-up table data. Both of these look-up tables are extracted from a benchmark test.

To improve the performance of original control strategy in real-time application, an optimal control strategy can be developed based on a novel MEC based cooperative control framework, where the mobile edge computing units (MECUs) at roadside can calculate the optimal thresholds for the control strategy based on the shared information, such as instantaneous velocities and geographical coordinates of the vehicles on the current route sector. With the shared information, the MECUs can predict the likely future vehicle velocity trajectory and optimize the control thresholds accordingly. This proposed MEC based cooperative control framework is shown in Fig. 3. In the development process of conventional energy management strategies, the thresholds that determine mode transition, including velocity boundaries and tractive power boundaries, and battery power limits in charge depleting and charge sustaining modes, are calibrated by hand according to the expert knowledge on some designated driving cycles. However, the limited expert knowledge is intractable to optimize the control effect, and the incomplete information hidden in calibrated driving cycles usually discounts the adaptability of the developed control strategy to varying traffic conditions in real-word scenarios. The predicated future velocity can inform the control unit of upcoming driving conditions in next route segment, thus supporting on-line adaptive control thresholds calibration by optimal algorithms and exhausting energy saving potential of PHEV. According to the forecasted velocity profile, the designed algorithm can optimize velocity boundaries and tractive power boundaries that are referred to for mode transition, as well as battery power constraints that can facilitate better different operation mode and energy consuming stage transition. In the proposed cooperative control framework, the MECU

that takes charge of any given route segment predicts the future velocity profiles for that route segment by the method described in [17]. Simultaneously, the specific MECU also optimally calculates the control thresholds in control strategy by CPSO-SQP for the driving in next route segment based on the predicted velocity profile of next segment. The forecasted velocity profile of vehicle driving in next segment is transmitted between MECUs via mmWave, which allows information about routes to be constructed. A global server assigns the MECUs according to the route to be travelled by the vehicle. The optimized control thresholds for vehicle driving in next route segment are issued to the on-board VCU from the MECU on duty. When the vehicle moves into next route segment, the on-board VCU updates the control strategy by employing the latest optimized control thresholds. Through the proposed optimization process, the optimal control thresholds can be determined for each segment before the vehicle enters it, enabling real-time optimal control. In addition to the specific designed control threshold optimization manner, the MEC based cooperative control framework also contributes to real-time implementation. Ref. [18] presents that the calculation capacity of on-board VCU in hybrid electric vehicles (HEVs) can reach 150 MIPS [18]; while as introduced in [19], the calculation capacity of the installed control unit in MECU can reach 955 MIPS, which is over 6 times higher than that in conventional on-board VCU, thus solidly underpinning complex real-time computation.

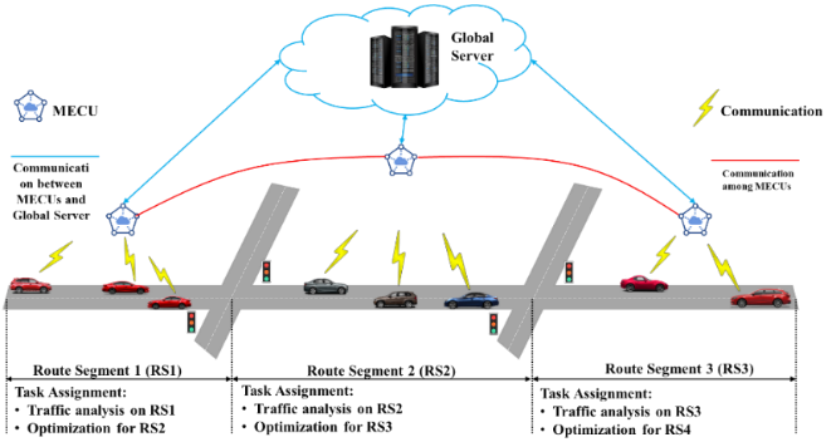

Fig. 3. The schematic of MEC based optimization.

III. CPSO-SQP Based Control Threshold Optimization

3.1 Particle Swarm Optimization (PSO)

PSO is a widely accepted evolutionary computational method [20] which can search for the optimal solution in multi-dimensional space by updating the particle position. In a population, each particle represents a solution

of the optimization problem, and it updates its position according to both its own and its 'neighbors' experience. The particle status can be generally characterized by particle position and velocity. The relationship between particle position and velocity can be expressed, as:

$$\begin{cases} V_i[t+1] = \omega V_i[t] + c_1\varphi(P_{besti} - X_i) + c_2\psi(P_{gbest} - X_i) \\ X_i[t+1] = X_i[t] + V_i[t+1] \end{cases} \quad (1)$$

where $V_i = [v_{i1}, v_{i2}, \ldots, v_{in}]$ is the velocity of particle i, $X_i = [x_{i1}, x_{i2}, \ldots, x_{in}]$ denotes the position of particle i, P_{besti} represents the best position of particle i, P_{gbest} is the optimal position among particles, φ and ψ are the uniformly distributed random variables, c_1 and c_2 are the acceleration coefficients, and ω is the inertial weight. The PSO has been applied in many fields [21]. However, given the nature of the searching process, it is possible that local, rather than global, optima may be identified, reducing the effectiveness of the approach.

3.2 Chaotic Particle Swam Optimization with Sequential Quadratic Programming

To avoid being trapped in local optima, the chaotic PSO with sequential quadratic programming (CPSO-SQP) is employed. This is a two-phased iterative strategy based on PSO [22]. The chaotic local search (CLS) is applied to reinforce the local oriented optimization, while the SQP is used to tune the search results [23]. The pseudo code of the CPSO-SQP is provided in Table 3.

Table 3 Pseudo Code of CPSO-SQP

1	**for** i=1 to *N* **do**
2	parameter initialization
3	**end**
4	**for** n=1 to iteration limit **do**
5	**for** i=1 to *N* **do**
6	$\begin{cases} V_i[t+1] = \omega V_i[t] + c_1\varphi(P_{besti} - X_i) + c_2\psi(P_{gbest} - X_i) \\ X_i[t+1] = X_i[t] + V_i[t+1] \end{cases}$
7	**do** *CLS*
8	**end**
9	**if** $P_{besti} < P_{best(i-1)}$ **then**
10	solve the optimization problem by SQP with start point of P_{besti}
11	**end**
12	**end**

The CLS is performed based on the Tent equation [21], as:

$$cx_i^{(k+1)} = \begin{cases} 2cx_i^{(k)}, 0 < cx_i^{(k)} \le 0.5 \\ 2(1 - 2cx_i^{(k)}), 0.5 < cx_i^{(k)} < 1 \end{cases} \quad (2)$$

where cx_i means the i th chaotic variable, and k denotes the iteration number. The procedure of CLS can be described as:

1. Initiate $k=0$, and convert the $x_i^{(k)}, i=1,2,\ldots,n$ within $(x_{min,i}, x_{max,i})$ to chaotic variable $cx_i^{(k)}$ in (0,1) by:

$$cx_i^{(k)} = \frac{x_i^k - x_{min,i}}{x_{max,i} - x_{min,i}} \tag{3}$$

2. Calculate $cx_i^{(k+1)}$ for next iteration by (2).

3. Convert $cx_i^{(k+1)}$ to $x_i^{(k+1)}$ by:

$$x_i^{(k+1)} = x_{min,i} + cx_i^{(k+1)}(x_{max,i} - x_{min,i}) \tag{4}$$

4. Evaluate the new solutions with $x_i^{(k+1)}, i=1,2,\ldots,n$

5. If the new solution is more optimal than $X^{(0)} = [X_1^{(0)}, X_2^{(0)}, \ldots, X_n^{(0)}]$ or iteration limits, output the new solution, or return to step 2.

The SQP has been verified capable in producing accurate solutions for nonlinear control problems with efficient performance [24]. In the iterative process, the Hessian of the Lagrangian function with the quasi-Newton update method is used to find the approximation to generate a quadratic programming (QP) sub-problem, which forms a search direction for the line optimization. The QP sub-problem can be formulated as:

$$\min \nabla F_T P_k^T d_k + \frac{1}{2} d_k^T H_k d_k \tag{5}$$

subject to:

$$C(P_k) + \nabla C(P_k)^T d_k = 0 \tag{6}$$

$$P_{min} \le P_k + d_k \le P_{max} \tag{7}$$

where H_k is the Hessian matric at the k th iteration, d_k represents the search direction, P_k denotes the optimal solution, $C(P_k)$ means the constraint in the optimization, and F_T is the cost function value. The relationship between F_T and $C(P_k)$ can be written as:

$$L(P,\lambda) = F_T(P) + C(P_k)^T \lambda \tag{8}$$

where λ is the Lagrangian multiplier vector. The quasi-Newton updating can be expressed, as:

$$H_{k+1} = H_k + \frac{Q_k Q_k^T}{Q_k^T S_k} - \frac{H_k^T S_k^T S_k H_k}{S_k^T H_k S_k} \tag{9}$$

where

$$S_k = P_{k+1} - P_k \tag{10}$$

$$Q_k = \nabla L(P_{k+1}, \lambda_{k+1}) - \nabla L(P_k, \lambda_{k+1}) \tag{11}$$

In each iteration of QP, the solution is utilized to form a new iteration, as:

$$P_{k+1} = P_k + \alpha_k d_k \tag{12}$$

where α_k is the step length applied to generate a reduction in the augmented Lagrangian function, such that:

$$L_A(P, \lambda, \rho) = F_T(P) - \lambda^T(P) + \frac{\rho}{2} C(P) C(P) \tag{13}$$

where ρ is a non-negative scalar. In the control threshold optimization by the CPSO-SQP, the updated particles are the control thresholds in the control strategy. The evaluation function J in each iteration can be written as:

$$J = \sum_{t=1}^{N} (\dot{m}_f(X) + \omega_t \frac{P_{batt}(X)}{Q_{lhv}}) \tag{14}$$

where $\dot{m}_f$ is the instant fuel consumption after determining the optimized control thresholds X on the particularly route segment, P_{batt} is the battery power, Q_{lhv} is the fuel low heat value, ω_t denotes the weighting on energy consumption, and t is the time step. The optimized control thresholds include variables that determine the mode transition and battery power limits in different operation modes in charge-depleting and charge-sustaining stage. The inequality constraints on the optimization problem can written as:

$$\begin{cases} SOC_{\min} \le SOC \le SOC_{\max} \\ P_{batt\_\min} \le P_{batt} \le P_{batt\_\max} \\ T_{eng\_\min} \le T_{eng} \le T_{eng\_\max} \\ T_{mot\_1\_\min} \le T_{mot1} \le T_{mot\_1\_\max} \\ T_{mot\_2\_\min} \le T_{mot2} \le T_{mot\_2\_\max} \\ T_{gen\_\min} \le T_{gen} \le T_{gen\_\max} \\ \omega_{eng\_\min} \le \omega_{eng} \le \omega_{eng\_\max} \\ \omega_{mot\_1\_\min} \le \omega_{mot\_1} \le \omega_{mot\_1\_\max} \\ \omega_{mot\_2\_\min} \le \omega_{mot\_2} \le \omega_{mot\_2\_\max} \\ \omega_{gen\_\min} \le \omega_{gen} \le \omega_{gen\_\max} \end{cases} \tag{15}$$

where the superscripts *min* and *max* denote the minimum and maximum value of each variable, respectively; T_{eng}, T_{mot_1}, T_{mot_2} and T_{gen} represent torque of ICE, motor 1, motor 2, and generator, respectively; and ω_{eng}, ω_{mot_1}, ω_{mot_2} and ω_{gen} denote their respective speeds. I_{batt} denotes the battery current. The maximum tractive torque that can be provided from powertrain is calculated according to the calibrated driver torque look-up table.

IV. AIOA Based Communication Ability Optimization

In general, IoV based MEC needs tree stages. The first stage is that the vehicles need to upload the data to the server by wireless communication, and then the server calculates the received tasks. Finally, the server returns the calculation results to the vehicles. It is assumed that IoVs adopt the mmWave communication because of its ultra-wide band. To mitigate hardware complexity and energy consumption, the base station (BS) and vehicles are equipped with single radio frequency (RF) chain, that can connect to multiple antennas via phase shifters (PSs) [16], as shown in Fig. 4.

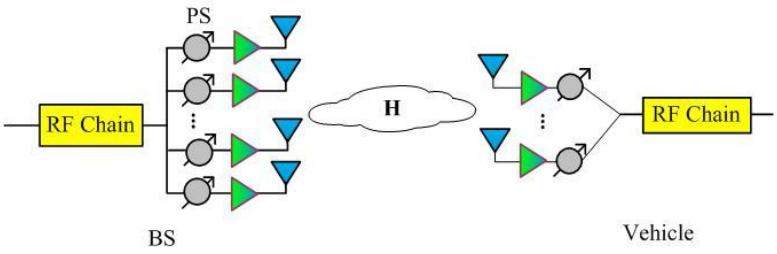

Fig. 4. The antenna structure at the BS and vehicle.

In addition, the BS and each vehicle are equipped with N and M ($M \le N$) antennas, respectively; and the BS is connected to the MEC via a highspeed backhaul link. The channel between the BS and each vehicle is assumed as flat fading, and the total mmWave bandwidth is set as B GHz. For avoiding the interference, each vehicle is allocated to a unique bandwidth. We assume that each BS can serve K vehicles according to its coverage area, and the allocated bandwidth for the kth vehicle is B_k, and thus, we have $\sum_{k=1}^{K} B_k \le B$。Therefore, the signal of the kth vehicle received by the BS can be expressed as:

$$y_k = \sqrt{p_k}\mathbf{f}\mathbf{H}_k\mathbf{g}_k x_k + \mathbf{f}_k\mathbf{n}_k \tag{16}$$

where $\mathbf{f}$ denotes the analog combine vector of the BS for all vehicles, $\mathbf{g}_k$, x_k and p_k represent the transmit precoding, transmit signal and transmit power of the kth vehicle, respectively. $\mathbf{H}_k$ denotes the mmWave channel

matrix between the BS and *k*th vehicle, and $\mathbf{n}_k$ is the received noise vector. For the mmWave channel, the widely used limited-scattering model is adopted with a uniform liner array [15], such that (we omit the index *k* here):

$$\mathbf{H} = \sum_{l=1}^{L} \alpha_l \mathbf{a}_t(\theta_l)\mathbf{a}_r^H(\phi_l) \tag{17}$$

where L denotes the number of multiple paths, α_l is the complex gain of the l th path, θ_l and ϕ_l denote the angle of arrival and angle of departure of the l th path, respectively. Therefore, the steering vectors $\mathbf{a}_t(\theta_l)$ and $\mathbf{a}_r(\phi_l)$ can be formulated, as:

$$\mathbf{a}_t(\theta_l) = \frac{1}{\sqrt{M}}\left[1, e^{j\pi\theta_l}, e^{j2\pi\theta_l}, ..., e^{j(M-1)\pi\theta_l}\right]^T \tag{18}$$

$$\mathbf{a}_r(\phi_l) = \frac{1}{\sqrt{N}}\left[1, e^{j\pi\phi_l}, e^{j2\pi\phi_l}, ..., e^{j(N-1)\pi\phi_l}\right]^T \tag{19}$$

According to the above analysis, the transmission rate of *k*th vehicle can be calculated, as:

$$R_k = B_k \log_2\left(1 + \frac{p_k \left|\mathbf{f}\mathbf{H}_k\mathbf{g}_k\right|^2}{\delta^2}\right) \tag{20}$$

where δ^2 deotes the noise power. It is assumed that there are A_k bits to be processed for the *k*th vehicle. Although the vehicle owns the computational resources and can execute the calculation task locally, the computational duration may be intensive due to the limited onboard computation capacity. Therefore, to reduce the system delay, the task can be partially offloaded to the BS and executed via the MEC server [25]. $\varsigma_k \in [0,1]$ denotes the task offloading ratio for the *k*th vehicle, and thus, $\varsigma_k A_k$ bits are offloaded to the BS and processed by the MEC server, while the *k*th vehicle executes the remaining $(1-\varsigma_k)A_k$ bits locally. Based on the findings in [26], it can be assumed that both the computational time on the MEC server at the BS and the feedback delay can be reasonably neglected. The offloaded computational delay includes two parts: the local computing delay and the transmission delay. If λ_k denotes the local computing resource of the *k*th vehicle, the computing delay can be expressed as:

$$T_k^c = \frac{(1-\varsigma_k)A_k}{\lambda_k} \tag{21}$$

Then, the transmission delay can be formulated, as:

$$T_k^t = \frac{\varsigma_k A_k}{R_k} \tag{22}$$

After that, the delay used to process A_k bits data can be expressed as:

$$T_k = \max\{T_k^c,\ T_k^t\} \tag{23}$$

Meanwhile, for guaranteeing the fairness among vehicles, the offloading computing delay minimization problem can be formulated, as:

$$\begin{aligned} &\min_{\{\mathbf{f},\mathbf{g}_k,\varsigma_k,B_k\}} \ \max_{\forall k}\ \{T_k\} \\ &s.t.\ \ \varsigma_k \in [0,1], k \in \{1,\ldots,\ K\} \\ &\quad \sum\nolimits_{k=1}^{K} B_k \le B \\ &\quad \left|\mathbf{f}(n)\right| = \frac{1}{\sqrt{N}}, n \in \{1,\ldots,\ N\},\ \left|\mathbf{g}_k(m)\right| = \frac{1}{\sqrt{M}}, m \in \{1,\ldots,\ M\} \end{aligned} \tag{24}$$

where $\mathbf{f}(n)$ and $\mathbf{g}_k(m)$ denote the nth element of $\mathbf{f}$ and the mth element of $\mathbf{g}_k$, respectively. The objective of (24) is to minimize the maximum delay among all the vehicles by jointly optimizing the transmit precoding $\mathbf{g}_k$, combine vector $\mathbf{f}$, the task offloading ratio ς_k and the bandwidth allocation B_k. In fact, it is extremely difficult to directly solve (24), and next an effective algorithm is proposed to tailor it. For each vehicle, it is obvious that the delay is minimum when the computing delay is equal to the transmission delay, i.e., $T_k^c = T_k^t$, such that we can obtain ς_k, as:

$$\varsigma_k = \frac{R_k}{R_k + \lambda_k}, k \in \{1,\ldots,K\} \tag{25}$$

By substituting ς_k into (24), the following optimization problem can be yielded, as:

$$\begin{aligned} &\min_{\{\mathbf{f},\mathbf{g}_k,B_k\}} \ \max_{\forall k}\ \frac{A_k}{B_k \log_2(1+\gamma_k) + \lambda_k} \\ &s.t. \sum\nolimits_{k=1}^{K} B_k \le B, \\ &\quad \left|\mathbf{f}(n)\right| = \frac{1}{\sqrt{N}}, n \in \{1,\ldots,\ N\}, \\ &\quad \left|\mathbf{g}_k(m)\right| = \frac{1}{\sqrt{M}}, m \in \{1,\ldots,\ M\} \end{aligned} \tag{26}$$

where the signal noise ratio (SNR) $\gamma_k = \frac{p_k \left|\mathbf{f}\mathbf{H}_k\mathbf{g}_k\right|^2}{\delta^2}$. It is obvious that (26) is still difficult to solve, and we define the spectral efficiency of the *k*th vehicle as $\log_2(1+\gamma_k)$. From (26), one can observe that the delay can be reduced for larger γ_k. Therefore, we consider maximizing the spectral efficiency of each vehicle and ignoring the transmission bandwidth, i.e.,

$$\begin{aligned} &\max_{\{\mathbf{f},\mathbf{g}_k\}} \quad \log_2\left(1+\gamma_k\right) \\ &s.t. \left|\mathbf{f}(n)\right| = \frac{1}{\sqrt{N}}, n \in \{1,\ldots,\ N\}, \\ &\quad \left|\mathbf{g}_k(m)\right| = \frac{1}{\sqrt{M}}, m \in \{1,\ldots,\ M\} \end{aligned} \tag{27}$$

According to (27), all the vehicles share the combine vector $\mathbf{f}$ of the BS. To reduce the complexity and guarantee the fairness, we assume that the antennas of BS are allocated in *K* sub-antenna sets, and each set includes $N^{'} = N / K$ antenna (we assume that $N^{'}$ is an integer, and when it is not an integer, we can adjust the antenna number). Next, $\mathbf{f} = [\mathbf{f}_1\ \mathbf{f}_2 \ldots \mathbf{f}_K]$ is defined, where $\mathbf{f}_k$ is a $1 \times N^{'}$ combine vector used for the *k*th vehicle. Then, Eqn. (27) can be divided into *K* individual sub-problems, as:

$$\begin{aligned} &\max_{\{\mathbf{f}_k,\mathbf{g}_k\}} \quad \log_2\left(1+\frac{p_k\left|\mathbf{f}_k\hat{\mathbf{H}}_k\mathbf{g}_k\right|^2}{\delta^2}\right) \\ &s.t. \left|\mathbf{f}_k(n)\right| = \frac{1}{\sqrt{N}}, n \in \{1,\ldots,\ N\}, \\ &\quad \left|\mathbf{g}_k(m)\right| = \frac{1}{\sqrt{M}}, m \in \{1,\ldots,\ M\} \end{aligned} \tag{28}$$

where $\hat{\mathbf{H}}_k$ denotes the sub-channel between the sub-antenna of the BS and vehicle. To solve (28), an alternatively iterative algorithm is proposed. Firstly, the analog transmit precoding $\mathbf{g}_k^o$ is initialized; then the analog combined vector can be directly yield, as:

$$\mathbf{f}_k^o(n) = \frac{\mathbf{h}_k(n)}{\sqrt{N\mathbf{h}_k^*(n)\mathbf{h}_k(n)}}, n \in \{1,\ldots N\} \tag{29}$$

where $\mathbf{h}_k = \hat{\mathbf{H}}_k\mathbf{g}_k^o$ and $\mathbf{f}_k^o(n)$ denotes the *n*th element of vector $\mathbf{f}_k^o$. Then, $\mathbf{f}_k^o$ is substituted into (28), and the value of the analog transmit precoding $\mathbf{g}_k^o$ is recalculated, as:

$$\mathbf{g}_k^o(m) = \frac{\mathbf{s}_k(m)}{\sqrt{M\mathbf{s}_k(m)\mathbf{s}_k^*(m)}},\ m \in \{1,\ldots,M\} \tag{30}$$

where $\mathbf{s}_k = \mathbf{f}_k^o \hat{\mathbf{H}}_k$. The calculation is repeated until convergence, and we define the final combined vector and transmitted precoding as $\mathbf{f}_k^{\text{opt}}$ and $\mathbf{g}_k^{\text{opt}}$. After that, the combined vector of the BS can be attained, as $\mathbf{f}^{\text{opt}} = [\mathbf{f}_1^{\text{opt}}, \mathbf{f}_2^{\text{opt}}, \ldots, \mathbf{f}_K^{\text{opt}}]$, and then $\mathbf{f}^{\text{opt}}$ and $\mathbf{g}_k^{\text{opt}}$ are substituted into (26). Thus, the bandwidth allocation optimization problem can be reformulated, as:

$$\begin{aligned} &\min_{\{B_k\}} \ \max_{\forall k} \ \frac{A_k}{B_k \log_2(1+\gamma_k) + \lambda_k} \\ &s.t. \sum_{k=1}^{K} B_k \le B \end{aligned} \tag{31}$$

To solve (31), we introduce auxiliary π and transform the original problem, as:

$$\begin{aligned} &\min_{\{B_k, \pi\}} \ \pi \\ &s.t. \sum_{k=1}^{K} B_k \le B \\ &\quad B_k \log_2(1+\gamma_k) + \lambda_k \ge \frac{A_k}{\pi}, k \in \{1,\ldots,K\} \end{aligned} \tag{32}$$

It is clear that (32) is a convex optimization problem and can be directly solved by the CVX toolbox. After obtaining the optimal bandwidth B_k for the *k*th vehicle, we can get the optimal task offloading ratio, as:

$$\varsigma_k = \frac{B_k \log_2(1+\gamma_k)}{B_k \log_2(1+\gamma_k) + \lambda_k}, k \in \{1,\ldots,K\} \tag{33}$$

V. Simulation and Evaluation

In the simulation evaluation, the original control strategy of a 4WD PHEV, which was developed through a series of standalone benchmark tests, is evaluated for potential improvements by leveraging IoV capability. In the simulation and evaluation, OS represents the original control strategy that is developed on the basis of rule logics, and OCS denotes the optimal control strategy based on IoV which has been proposed in this paper. The optimization of the control strategy based on dynamic programming (DP) is also presented for benchmark. The detailed parameters of the 4WD PHEV are provided in Table 4, and the simulation is conducted on a workstation with an Intel Xeon E3-1270 @ 3.4 GHz and 32 Gigabytes memory. In the simulation, the performance of the raised method in communication optimization and optimal control is comprehensively evaluated.

Table 4 Component Parameters in the 4WD PHEV

Engine	**Displacement**	**2.0 [L] 16V DOHC**
	Maximum Power	89 [kW] @4500 [rpm]
	Maximum Torque	190 [Nm] @4500 [rpm]
Motor 1	Maximum Power	60 [kW]
	Maximum Torque	137 [Nm]
Motor 2	Maximum Power	60 [kW]
	Maximum Torque	195 [Nm]
Battery	Type	Lithium-ion
	Capacity	12 [kWh]
	Nominal Voltage	300 [V]
Gear Ratio	Between ICE and final drive	i_{g1}=3.425
	Between motor 1 and final drive	i_{g2}=9.663
	Between motor 2 and final drive	i_{g3}=7.065
	Between ICE and generator	i_{g4}=2.736

4.1 Performance Evaluation of the Raised Method in Communication Improvement

Figs. 5 to 8 show the results of our proposed algorithm. We assume that the number of vehicles within the serving area of certain MECU is $K=5$, and $M=4$ antennas are deployed in each vehicle. For convenience, we assume that the local computing capabilities, processed data size and transmit power for each vehicle remain the same, i.e., $\lambda_1=\lambda_2=\cdots=\lambda_K=\lambda$, $A_1=A_2=\cdots=A_K=A$, and $p_1=p_2=\cdots=p_K=p$. The BS antennas is $N=60$, and the signal-to-noise ratio (SNR) equals p/δ^2 after calculation. The total size of computational task is $A=100$ Mbit/s, the local computing capability is $\lambda=1$ Gbit/s, and the total bandwidth is $B=10$ GHz. Fig. 5 shows the convergence trend of the proposed algorithm when solving (28). It is obvious that the spectral efficiency speedily converges to a stable value, manifesting the effectiveness of the proposed algorithm. The spectral efficiency obtained by BS differs for different vehicles, due to the random channel condition between each vehicle and BS.

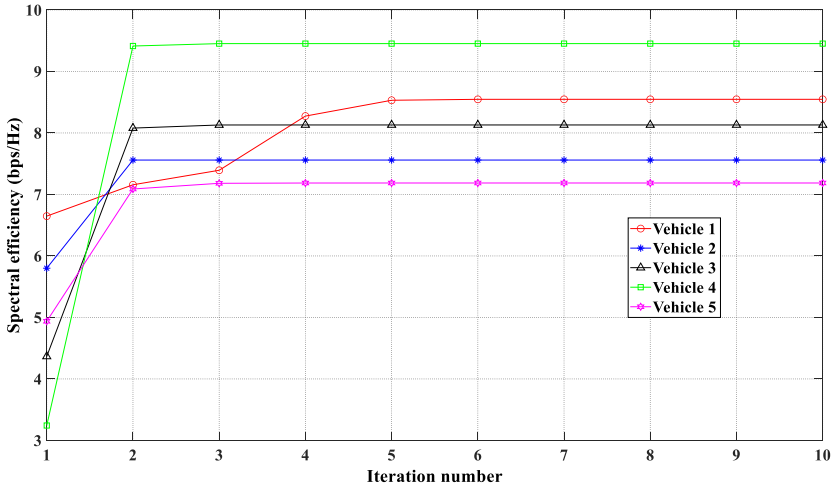

Fig. 5. The convergence for the proposed alternatively iterative algorithm.

Fig. 6 shows the delay under different bandwidths, where we set the total bandwidth as 10 GHz, 15 GHz and 20 GHz, respectively. One can observe that the delay decreases with the increase of bandwidth for the same SNR. This is because when the bandwidth increases, the transmission rate will be improved, as calculated in (20). As a result, the transmission delay calculated in (22) will be reduced. On the other hand, it can also be found that the delay decreases with the increase of SNR. This is also easy to understand that larger SNR can raise higher transmission rate, which also mitigates the transmission delay. In addition, we can find that the delay is always limited within 10 ms, which is enough for controlling vehicles. Fig. 7 shows the delay versus SNR under different local computing capacities, where we set local computing capacity λ as 1 Gbits/s, 2 Gbits/s and 3 Gbits/s, respectively. It is obvious that lower delay leads to more local computing capacity. It is also easy to understand that the processed data can be finished quickly when the computing capacity of a server is enough. Additionally, the same conclusion can be attained that the delay decreases with the increase of SNR. The bandwidth allocation result for each vehicle is plotted in Fig. 9. One can observe that different vehicles are allocated to different bandwidth, as the channel vector of each vehicle is different and thus results in different channel gains. Therefore, when the channel gain of the vehicle is low, it will be allocated to more bandwidth to improve the transmission rate and reduce the delay. The results illustrated in Figs. 5 to 8 validate that the optimized communication delay allows that the cooperation within the MEC based framework can be performed freely, and the prompted communication speed in V2V and V2I promotes the efficiency of raised novel method in real-time application.

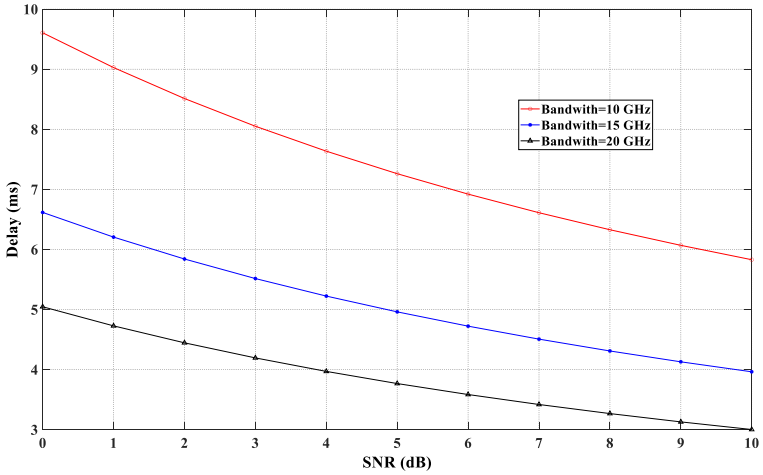

Fig. 6. The delay versus SNR under different bandwidth.

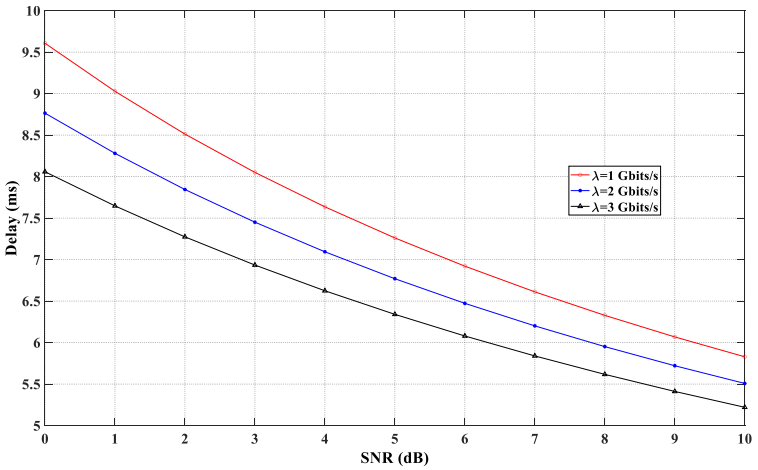

Fig. 7. The delay versus SNR under different local computing capacities.

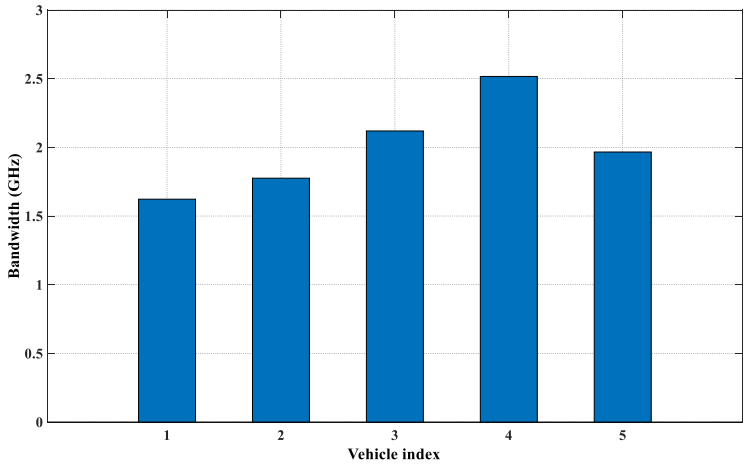

Fig. 8. The bandwidth allocation for each vehicle.

4.2 Assessment on the Effectiveness of the Novel Control Strategy

Fig. 9 (a) shows the predicted fuel consumption of the 4WD PHEV using three different strategies. The IoV enables enhanced adaptability to different driving conditions, thus resulting in better selection of operational mode and distribution energy between the available power sources. The fuel consumption predicted by the optimal control strategy is closer to that of DP across a number of cycle segments (such as 1000 s to 1500 s and 6000 s to 7500 s) and throughout the trip as a whole trip. The control threshold optimization in each route segments delivers control decisions are close, or equal, to those that would have been identified by DP. Fig. 9 (b) shows the effect on the battery SOC by different methods. The optimal strategy regulates the SOC to decrease in slow, continuous rates, rather than the relatively large discharge outputted by the original control strategy. The slower discharge of the battery SOC coupled with the reduced fuel consumption results reinforces that the energy management in the vehicle can be managed better. Similar to the fuel consumption results, the battery SOC profile is closer to that predicted by DP. Table 5 lists the detailed fuel consumption results. The equivalent fuel consumption of the new

optimal control strategy, including the converted equivalent fuel consumption from the electric energy, is closer to that of DP. The normalized average performance of optimally designed method is 98.4% of that by DP, where the values obtained through the DP can be considered as the 'ideal' case.

Table 5 Compare in Fuel Consumption.

Strategy	Fuel Consumption (g)	Converted Fuel Consumption (L/100km)	Normalized Average value
OS	3439	4.22	89.5%
OCS	3121	3.84	98.4%
DP	3077	3.78	100%

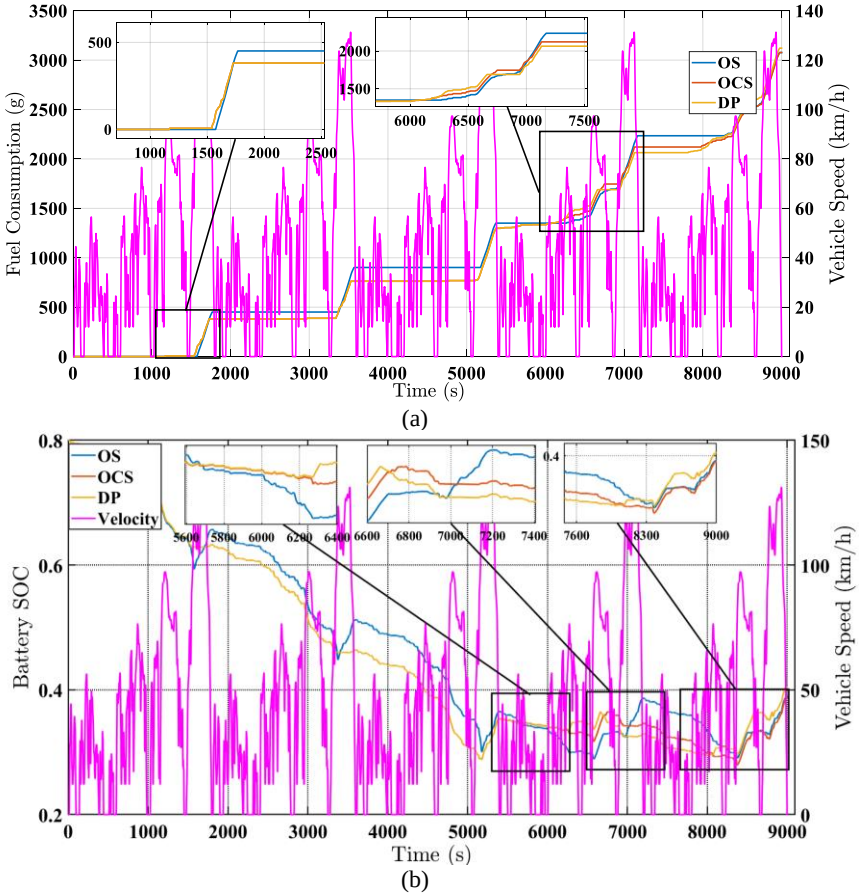

Fig. 9. The energy consumption by different methods. (a) Engine fuel consumption; (b) Electric energy consumption reflected by battery SOC.

Figs. 10 (a) to (c) illustrate the engine operational points. In the original control strategy, these points are more dispersed, compared with those by the optimal control strategy and DP. In addition, most of the engine operation points identified by the optimal control strategy and DP are located in the high efficiency region. Fig. 11 (a) shows the generator torque during simulation. Despite the operation mode, the operation points of the generator by the optimal control strategy and DP are more concentrated than those by the original control strategy, proving the rational performance of the optimal control strategy from another perspective, as the generator

operation is highly correlated with the engine operation. By observing Figs. 11 (a) to (c) as a whole, it can be found that the optimized control thresholds promote more stable operation with less mode transition and overall better fuel economy for the studied PHEV.

Table 6 Compare in Engine Operation Time

Strategy	**OS**	**OCS**	**DP**
Engine Operation Time (s)	1753	1543	1485

Figs. 11 (b) and (c) provide further insight into the engine and generator operation. A number of cycle segments (such as 6000 s to 7500 s in Fig. 11 (b) and 5500 s to 7500 s in Fig. 11 (c)) shows the tight cooperation between ICE and generator. The optimized control strategy in this paper governs the operation of ICE and generator optimally by avoiding frequent on/off. The control behaviors by the proposed method are closer to those by DP. Table 6 lists the engine operation times by three methods. In Table 6, the engine operation time by the optimal strategy is less than that by the original control strategy, demonstrating that the optimal strategy can better employ the electrical energy and improve the cooperation among the ICE, generator and motor.

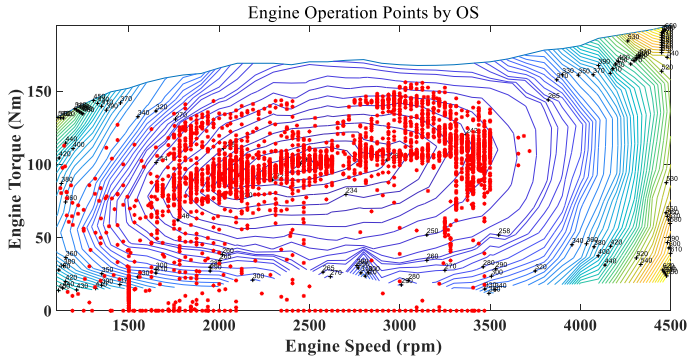

(a)

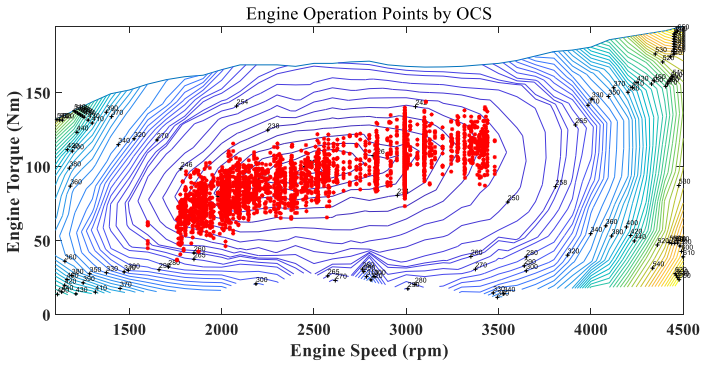

(b)

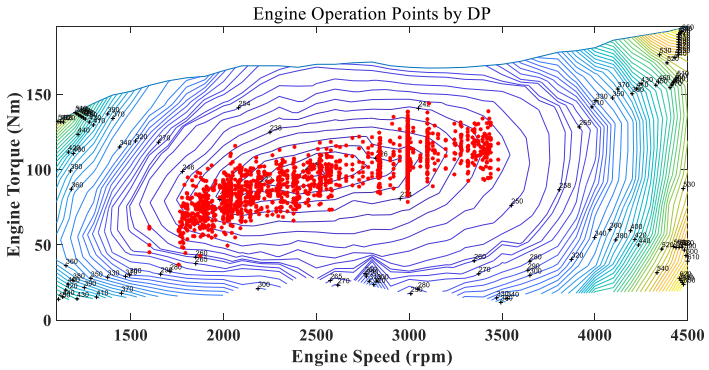

(c)

Fig. 10. The engine operation by different methods. (a) The engine operation by OS; (b) The engine operation by OCS; (c) The engine operation by DP.

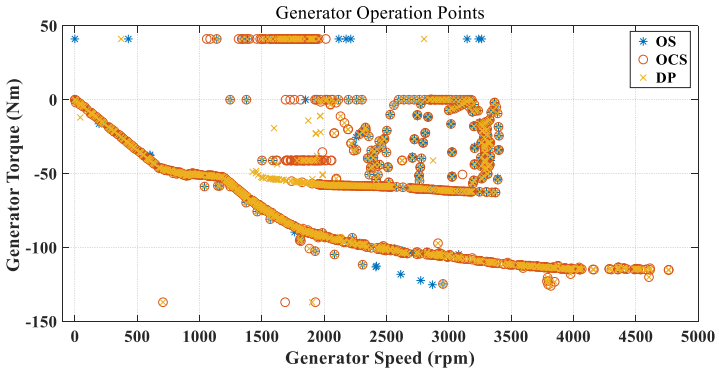

(a)

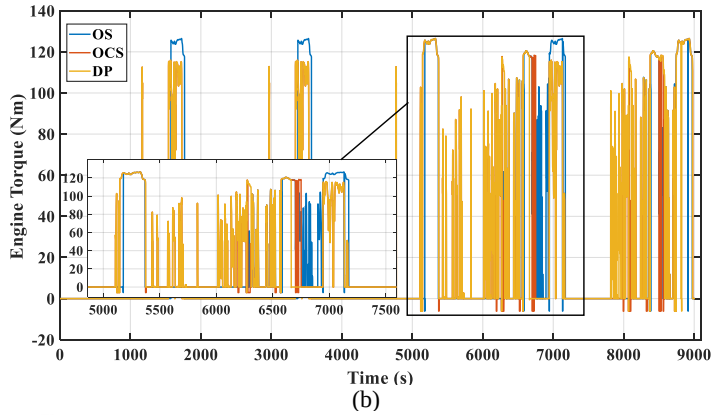

(b)

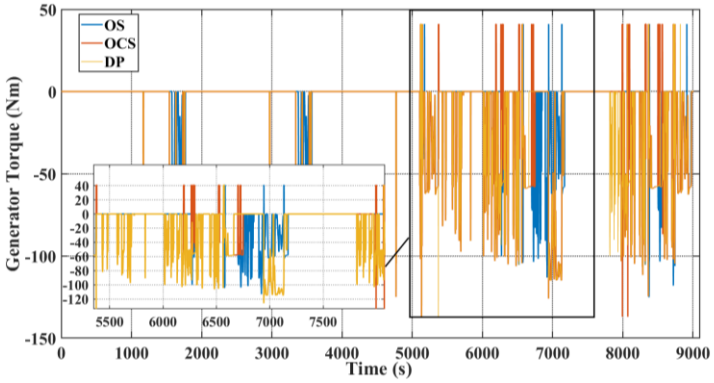

(c)

Fig. 11. Different components performance. (a) . Generator operation points by different methods in 5 WLTC cycles.; (b) Engine torques by different methods in 5 WLTC cycles; (c) Generator torques by different methods in 5 WLTC cycles.

In the simulation, the step computational time of the three different methods is also discussed to assess their real-time implementation ability. Table 7 lists the computing times of the three methods. During simulation, each MECU accounts for a route segment of 500 m length. The total computing time is the sum of the computing time in each route segment. The step computing time can be calculated by dividing the total computing time over total simulation steps. Note that the simulation step is 1s. Even though the step computing time of the optimal control strategy is a bit more than the original control strategy, the optimal control strategy can still complete the control process in one simulation step, justifying its online operation ability in real-time application. For the step computing time by DP, it is larger than the simulation step time, and thus it cannot be applied online.

Table 7 Compare in Step Computing Time.

Strategy	**OS**	**OCS**	**DP**
Step Computing Time (s)	0.0712	0.109	2.374

Through evaluation, it can be concluded the optimal control strategy proposed in this study can improve the performance of the simple rule based control strategy by enabling responsiveness to driving conditions through vehicle-environment cooperative control. Even though the advanced optimization method has been preferred, the complex optimization has never encroached the remarkable implementation ability of the raised method in real time after leveraging the MEC based framework.

V. CONCLUSION

The development of a framework optimal control of a 4-wheel plug-in hybrid electric vehicle using Internet of Vehicles is presented in this study. The control thresholds in the strategy are optimized by the chaotic particle optimization with sequential quadratic programming by virtue of the mobile edge computing-based framework. To guarantee the ideal control effect, the communication ability in the mobile edge computing-based framework is optimized by the alternatively iterative algorithm. The simulation results demonstrate that the method achieves better performance when compared with the original control strategy derived from benchmark testing. The fuel economy of the studied vehicle by the optimal control strategy can be improved by 9%. The control effect of the optimal control strategy can reach 98.4% of that by dynamic programming. The analysis in step computing time highlights the reasonable capability of the optimal control strategy in real-time application. The proposed novel control strategy provides a novel inspiration on improving vehicle performance from the perspective of vehicle-environment cooperative control. Owing to its specific control mechanism, the novel control strategy avoids the

burdensome computation in real time. With the assist from the advanced communication techniques, the novel control strategy holds significant potential in instant application and promotes the performance of plug-in hybrid electric vehicle dramatically.

In the future work, we will focus on the mobile edge computing based application. In addition, driving condition prediction methods in the framework of internet of vehicles will be studied, and novel vehicle-environment cooperative control methods will also be investigated.

ACKNOWLEDGEMENT

This work was supported in part by the National Natural Science Foundation of China (No. 61763021 and No. 51775063), in part by the National Key R&D Program of China (No. 2018YFB0104900), and in part by the EU-funded Marie Skłodowska-Curie Individual Fellowships Project under Grant 845102-HOEMEV-H2020-MSCA-IF-2018.

REFERENCE

[1] X. Cheng, C. Chen, W. Zhang, and Y. Yang, "5G-Enabled Cooperative Intelligent Vehicular (5GenCIV) Framework: When Benz Meets Marconi," IEEE Intelligent Systems, vol. 32, no. 3, pp. 53-59, May-Jun 2017.
[2] N. Abbas, Y. Zhang, A. Taherkordi, and T. Skeie, "Mobile Edge Computing: A Survey," IEEE Internet of Things Journal, vol. 5, no. 1, pp. 450-465, Feb 2018.
[3] Zhang, Yuanjian, et al. "A novel strategy for power sources management in connected plug-in hybrid electric vehicles based on mobile edge computation framework." Journal of Power Sources 477 (2020): 228650.
[4] Liu, Yonggang, et al. "Rule learning based energy management strategy of fuel cell hybrid vehicles considering multi-objective optimization." Energy 207 (2020): 118212.
[5] Hongwen, He, et al. "Real-time global driving cycle construction and the application to economy driving pro system in plug-in hybrid electric vehicles." Energy 152 (2018): 95-107.
[6] Tian, He, et al. "Data-driven hierarchical control for online energy management of plug-in hybrid electric city bus." Energy 142 (2018): 55-67.
[7] Y. Zhang et al., "Energy management strategy for plug-in hybrid electric vehicle integrated with vehicle-environment cooperation control," Energy, Article vol. 197, 2020, Art. no. 117192.
[8] Guo, Ningyuan, et al. "Real-time Predictive Energy Management of Plug-in Hybrid Electric Vehicles for Coordination of Fuel Economy and Battery Degradation." Energy (2020): 119070.
[9] Duan, Benming, et al. "Calibration methodology for energy management system of a plug-in hybrid electric vehicle." Energy Conversion and Management 136 (2017): 240-248.
[10] Gao, Dawei, Zhenhua Jin, and Qingchun Lu. "Energy management strategy based on fuzzy logic for a fuel cell hybrid bus." Journal of Power Sources 185.1 (2008): 311-317.
[11] Xie, Shaobo, et al. "Predictive vehicle-following power management for plug-in hybrid electric vehicles." Energy 166 (2019): 701-714.
[12] Chen, Zheng, et al. "Stochastic Model Predictive Control for Energy Management of Power-Split Plug-in Hybrid Electric Vehicles Based on Reinforcement Learning." Energy (2020): 118931.
[13] Tan, Huachun, et al. "Energy management of hybrid electric bus based on deep reinforcement learning in continuous state and action space." Energy Conversion and Management 195 (2019): 548-560.
[14] Y. Mao, C. You, J. Zhang, K. Huang, and K. B. Letaief, "A Survey on Mobile Edge Computing: The Communication Perspective," IEEE Communications Surveys and Tutorials, vol. 19, no. 4, pp. 2322-2358, 2017 2017.
[15] O. El Ayach, S. Rajagopal, S. Abu-Surra, Z. Pi, and R. W. Heath, Jr., "Spatially Sparse Precoding in Millimeter Wave MIMO Systems," IEEE Transactions on Wireless Communications, vol. 13, no. 3, pp. 1499-1513, Mar 2014.
[16] X. Gao, L. Dai, and A. M. Sayeed, "Low RF-Complexity Technologies to Enable Millimeter-Wave MIMO with Large Antenna Array for 5G Wireless Communications," IEEE Communications Magazine, vol. 56, no. 4, pp. 211-217, Apr 2018.
[17] Y. Zhang, L. Chu, Y. Ou, C. Guo, Y. Liu, and X. Tang, "A Cyber-Physical System-Based Velocity-Profile Prediction Method and Case Study of Application in Plug-In Hybrid Electric Vehicle," IEEE transactions on cybernetics, 2019-Aug-05 2019.

[18] Li, Weimin, et al. "Design of vehicle control unit based on DSP for a parallel HEV." 2007 IEEE International Conference on Automation and Logistics. IEEE, 2007.
[19] Lee, Juyong, Jeong-Weon Kim, and Jihoon Lee. "Mobile personal multi-access edge computing architecture composed of individual user devices." Applied Sciences 10.13 (2020): 4643.
[20] W.-B. Du, W. Ying, G. Yan, Y.-B. Zhu, and X.-B. Cao, "Heterogeneous Strategy Particle Swarm Optimization," IEEE Transactions on Circuits and Systems Ii-Express Briefs, vol. 64, no. 4, pp. 467-471, Apr 2017.
[21] I. Soesanti and R. Syahputra, "Batik production process optimization using particle swarm optimization method," Journal of Theoretical and Applied Information Technology, Article vol. 86, no. 2, pp. 272-278, 2016.
[22] C. Qi, A. Fourie, and Q. Chen, "Neural network and particle swarm optimization for predicting the unconfined compressive strength of cemented paste backfill," Construction and Building Materials, vol. 159, pp. 473-478, Jan 20 2018.
[23] T. A. A. Victoire and A. E. Jeyakumar, "Hybrid PSO-SQP for economic dispatch with valve-point effect," Electric Power Systems Research, vol. 71, no. 1, pp. 51-59, Sep 2004.
[24] P. E. Gill, W. Murray, and M. A. Saunders, "SNOPT: An SQP algorithm for large-scale constrained optimization," Siam Journal on Optimization, vol. 12, no. 4, pp. 979-1006, Apr 26 2002, Art. no. Pii s1052623499350013.
[25] J. Ren, G. Yu, Y. He, and G. Y. Li, "Collaborative Cloud and Edge Computing for Latency Minimization," IEEE Transactions on Vehicular Technology, vol. 68, no. 5, pp. 5031-5044, May 2019.
[26] P. Wang, C. Yao, Z. Zheng, G. Sun, and L. Song, "Joint Task Assignment, Transmission, and Computing Resource Allocation in Multilayer Mobile Edge Computing Systems," IEEE Internet of Things Journal, vol. 6, no. 2, pp. 2872-2884, Apr 2019.